AIAA Modeling and Simulation Technologies Conference and Exhibit
20 - 23 August 2007, Hilton Head, South Carolina

AIAA 2007-6706

Optimal Trajectories for Tethered Kite Mounted on a Vertical Axis Generator

Paul Williams,[*] Bas Lansdorp,[†] Wubbo Ockels[‡]
Delft University, The Netherlands

Tethered kite technology promises the enable the efficient extraction of energy from high altitude winds. One possible concept for converting the wind energy into electricity is to generate useful work at the ground by using a tether. The tether is able to drive a generator in one of two ways: either the tether is wound and unwound, or the tether is attached to a lever arm that creates a torque on the generator. The latter concept, which uses a vertical axis generator, is explored in this paper. A simplified dynamic model of the system is used to optimize the kite motion to give the maximum power generated per operating cycle. The results show that the average optimal power generated per cycle is proportional to the kite area and the cube of the wind speed. Experimental results of a remotely controlled kite are also briefly reviewed.

I. Introduction

HIGH altitudes are beneficial for energy production due to the average speed of the wind being much larger than at ground level.[1-3] However, it is not easy to extract energy from high altitudes due to construction costs associated with conventional wind energy systems, such as turbines. An alternative concept to placing a generator at high altitudes[3-19] is to attempt to mechanically drive a ground-based generator using an aerial system.[2] One such system is the Laddermill,[21-25] which proposes to use a train of kites on a cable. The kites are flown in a way that generates high tension, thereby pulling the cable off a drum, which in turn drives a generator. Changing the kite flight dynamics to reduce the tension when the cable is reeled in allows net energy to be produced over an operating cycle.[26-27] The Laddermill concept shows considerable promise. Ref. 27 demonstrated that the optimal power is generated by flying the kite across the wind,[28] which generates substantially more power than flying the kite within a single plane.[26]

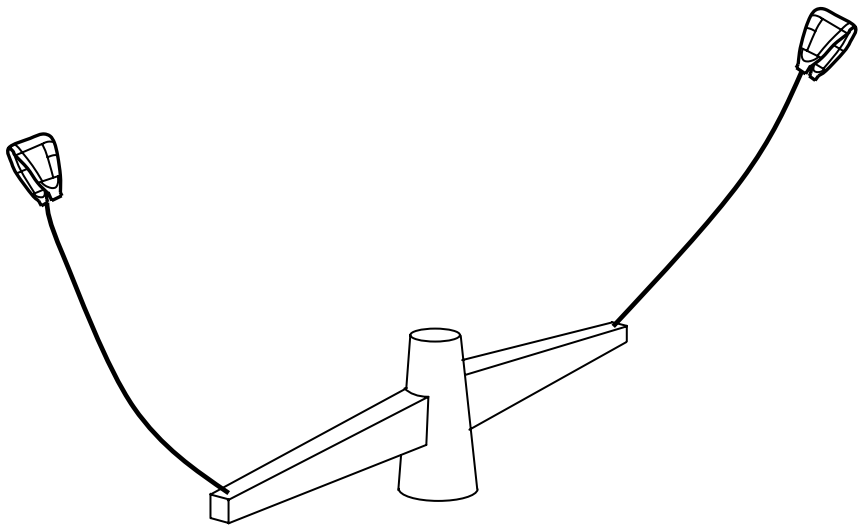

Fig. 1 Vertical axis wind generator concept with two kites.

[*] AIAA Member, e-mail: tethered.systems@gmail.com.
[†] PhD researcher, Faculty of Aerospace Engineering, E-mail: b.lansdorp@tudelft.nl.
[‡] ASSET Chairholder, Faculty of Aerospace Engineering, E-mail: w.j.ockels@tudelft.nl.

An alternative concept is to attach the cable to a lever arm on a vertical axis generator, as shown in Fig. 1. This concept uses the kite to continually fly in a manner that maximizes the torque or power at the ground generator. The system can utilize multiple lever arms and kites to increase the torque produced by the system. The vertical axis configuration can take advantage of the fact that the direction of rotation does not need to change. This should ensure uninterrupted power supply during normal operation. However, the disadvantage of this approach is that the tether needs to have a relatively large inclination to the vertical and be in a direction perpendicular to the lever arm to generate a torque on the system. Nevertheless, by proper control of the system it should be possible to generate significant energy.

This paper develops a simulation model of a vertical axis kite system for power generation. The purpose of the model is to enable the calculation of optimal trajectories for the system. The model is based on the assumption that the tether(s) remain straight. The tether(s) are capable of varying in length, but the kite is controlled by specifying the angle of attack and roll angle. The system dynamics are optimized to produce maximum power using numerical optimization techniques.

II. Dynamic Model of a Tethered Kite System on Rotating Base

To study the capability of generating continuous power using a vertical axis generator, we develop a simplified model that captures the effects of a maneuvering kite connected to a rotating base. For simplicity, we derive the case where one tether is connected to the system, but the extension to additional kites and tethers is straightforward. A representation of the system is shown in Fig. 2. The kite is modeled as a point mass with lift and drag forces. In this preliminary analysis, tether mass and drag are ignored, but these are relatively easy to incorporate. However, there presence tends to slow the computations, without significantly altering any major conclusions. Hence, for the sake of efficiency over precise accuracy, tether mass and drag are not included.

The main rotating base is assumed to have a rotational inertia denoted by J. The tether is connected to the system at a radius R from the center of rotation. An inertial coordinate frame is used which is attached to the center of the generator, O. The axes are defined such that the x-axis points in the direction of the wind, the z-axis points vertically upwards, and the y-axis completes the right-handed triad. The angle of rotation of the lever arm is denoted by γ, measured relative to the inertial x-axis. The position of the kite is obtained relative to the end of the lever arm by the angles θ and ϕ. The angle θ is measured relative to the vertical in the direction tangential to the lever arm, and the angle ϕ measures the displacement normal to the lever arm, positive in the direction of rotation.

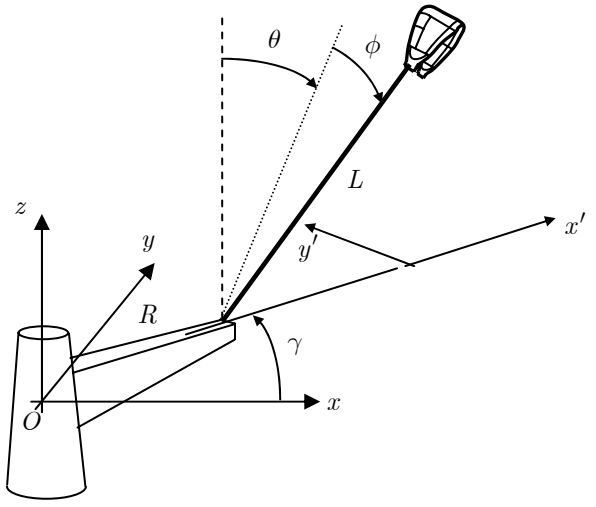

Fig. 2 Tethered kite system model.

Let the local lever arm axes be defined relative to the inertial axes as follows

$$\begin{bmatrix} x \\ y \\ z \end{bmatrix} = \begin{bmatrix} \cos\gamma & -\sin\gamma & 0 \\ \sin\gamma & \cos\gamma & 0 \\ 0 & 0 & 1 \end{bmatrix} \begin{bmatrix} x' \\ y' \\ z' \end{bmatrix} \tag{1}$$

The direction of the tether is defined in the local lever arm axis system as shown in Fig. 3. Hence, the direction of the tether may be written as

$$\boldsymbol{r} = [L\sin\theta\cos\phi, L\sin\phi, L\cos\theta\cos\phi] \tag{2}$$

The position of the tether tip in the rotating lever frame is given by

$$\boldsymbol{r}_k = [R + L\sin\theta\cos\phi, L\sin\phi, L\cos\theta\cos\phi] \tag{3}$$

where L is the tether length.

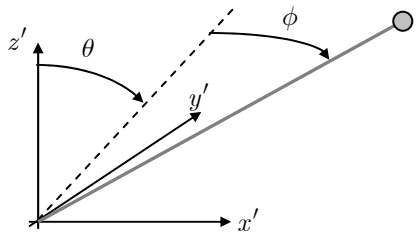

Fig. 3 Tether direction relative to the local lever arm.

Using the definition of the tether angles, the position of the kite in the inertial coordinate system is given by

$$\boldsymbol{R}_k = \begin{bmatrix} \cos\gamma & -\sin\gamma & 0 \\ \sin\gamma & \cos\gamma & 0 \\ 0 & 0 & 1 \end{bmatrix} \begin{bmatrix} R + L\sin\theta\cos\phi \\ L\sin\phi \\ L\cos\theta\cos\phi \end{bmatrix} \tag{4}$$

$$\boldsymbol{R}_k = [R\cos\gamma + L\sin\theta\cos\phi\cos\gamma - L\sin\phi\sin\gamma, R\sin\gamma + L\sin\theta\cos\phi\sin\gamma + L\sin\phi\cos\gamma, L\cos\theta\cos\phi] \tag{5}$$

The Lagrangian of the system is obtained as a combination of rotational energy due to the lever arm, translational energy from the kite, and potential energy from the kite. This can be expressed as

$$\mathcal{L} = \frac{1}{2}J\dot{\gamma}^2 + \frac{1}{2}m_k\dot{\boldsymbol{R}}_k \cdot \dot{\boldsymbol{R}}_k - m_k g L\cos\theta\cos\phi \tag{6}$$

The coupled equations of motion are derived using the standard form of Lagrange's equations as follows

$$\frac{\mathrm{d}}{\mathrm{d}t}\left(\frac{\partial\mathcal{L}}{\partial\dot{q}_j}\right) - \frac{\partial\mathcal{L}}{\partial q_j} = Q_{q_j} \tag{7}$$

The tether length is assumed to be a controlled input via the length acceleration $\ddot{L}$. Hence, the equation of motion that represents the variation in tether length is used to calculate the tension in the tether. This is important because the tension must be kept positive to avoid the tether becoming slack. A slack tether also invalidates the model since the length to the kite is no longer correct. Note that if tension is a control input, then the model will behave correctly for zero tension.

The equations of motion can be written in matrix form as follows

$$[M]\begin{bmatrix}\ddot{\gamma}\\ \ddot{\theta}\\ \ddot{\phi}\\ T\end{bmatrix} = B \tag{8}$$

$$M = \begin{bmatrix} J + m_k R^2 + m_k L^2 + 2m_k RL\sin\theta\cos\phi - m_k L^2\cos^2\phi\cos^2\theta & -m_k L^2\cos\theta\cos\phi\sin\phi & m_k L^2\sin\theta + m_k LR\cos\phi & 0\\ -m_k L^2\cos\theta\cos\phi\sin\phi & m_k L^2\cos^2\phi & 0 & 0\\ m_k L(R\cos\phi + L\sin\theta) & 0 & m_k L^2 & 0\\ m_k R\sin\phi & 0 & 0 & 1 \end{bmatrix} \tag{9}$$

$$\begin{aligned} B_\gamma &= Q_\gamma - m_k\ddot{L}R\sin\phi - 2m_k\dot{\gamma}L\dot{L} - 2m_k\dot{L}R\dot{\phi}\cos\phi - 2m_k R\dot{\gamma}\dot{L}\sin\theta\cos\phi - 2m_k R\dot{\gamma}\dot{\theta}L\cos\theta\cos\phi\\ &+2m_k R\dot{\gamma}\dot{\phi}L\sin\theta\sin\phi + 2m_k L\dot{L}\dot{\gamma}\cos^2\phi\cos^2\theta - 2m_k L^2\dot{\gamma}\dot{\phi}\cos\phi\cos^2\theta\sin\phi - 2m_k L^2\dot{\gamma}\dot{\theta}\cos^2\phi\cos\theta\sin\theta\\ &+m_k L\dot{\phi}^2 R\sin\phi + 2m_k L\dot{L}\dot{\theta}\cos\theta\cos\phi\sin\phi - m_k L^2\dot{\theta}^2\sin\theta\cos\phi\sin\phi - m_k L^2\dot{\theta}\dot{\phi}\cos\theta\sin^2\phi + m_k L^2\dot{\theta}\dot{\phi}\cos\theta\cos^2\phi\\ &-2m_k L\dot{L}\dot{\phi}\sin\theta - m_k L^2\dot{\theta}\dot{\phi}\cos\theta \end{aligned} \tag{10}$$

$$\begin{aligned} B_\theta &= m_k L^2\dot{\phi}\sin\phi(-\dot{\gamma}\cos\theta\sin\phi + \dot{\theta}\cos\phi) - 2m_k\dot{L}L\cos\phi(-\dot{\gamma}\cos\theta\sin\phi + \dot{\theta}\cos\phi)\\ &-m_k L^2\cos\phi(\dot{\theta}\dot{\gamma}\sin\theta\sin\phi - \dot{\phi}\dot{\gamma}\cos\theta\cos\phi - \dot{\theta}\dot{\phi}\sin\phi) + m_k L(g\sin\theta\cos\phi + R\dot{\gamma}^2\cos\theta\cos\phi + L\dot{\gamma}^2\sin\theta\cos^2\phi\cos\theta\\ &+L\dot{\gamma}\dot{\theta}\sin\phi\sin\theta\cos\phi + L\dot{\gamma}\dot{\phi}\cos\theta) + Q_\theta \end{aligned} \tag{11}$$

$$\begin{aligned} B_\phi &= -m_k\dot{L}(R\dot{\gamma}\cos\phi + L\dot{\phi} + L\dot{\gamma}\sin\theta) - m_k L(-R\dot{\gamma}\dot{\phi}\sin\phi + \dot{L}\dot{\phi} + \dot{L}\dot{\gamma}\sin\theta + L\dot{\gamma}\dot{\theta}\cos\theta)\\ &-m_k(-gL\cos\theta\sin\phi + R\dot{\gamma}^2 L\sin\theta\sin\phi - R\dot{\gamma}\dot{L}\cos\phi + R\dot{\gamma}\dot{\phi}L\sin\phi - L^2\dot{\gamma}^2\cos\phi\sin\phi\cos^2\theta\\ &+2L^2\dot{\theta}\dot{\gamma}\cos\theta\cos^2\phi - L^2\dot{\theta}\dot{\gamma}\cos\theta + L^2\dot{\theta}^2\cos\phi\sin\phi) + Q_\phi \end{aligned} \tag{12}$$

$$\begin{aligned} B_T &= -m_k(\ddot{L} + R\dot{\gamma}\dot{\phi}\cos\phi) + m_k(-g\cos\theta\cos\phi + L\dot{\gamma}^2 + L\dot{\theta}^2\cos^2\phi + L\dot{\phi}^2 - L\dot{\gamma}^2\cos^2\phi\cos^2\theta\\ &+R\dot{\gamma}^2\sin\theta\cos\phi + R\dot{\gamma}\dot{\phi}\cos\phi + 2L\dot{\phi}\dot{\gamma}\sin\theta - 2L\dot{\theta}\dot{\gamma}\cos\theta\cos\phi\sin\phi) + Q_L \end{aligned} \tag{13}$$

The generalized forces that appear in Eqs. (10) through (13) arise from the lift and drag forces on the kite, as well as the resistance created as the generator extracts energy from the system. These forces must be included in the model to enable the system to be simulated. It should be noted that the model derived is quite general and can also be used to simulate a static base kite system, i.e., by setting $\dot{\gamma} = 0$. For efficient implementation, it is possible to analytically solve for the second derivatives of the generalized coordinates in Eq. (8). However, the resulting equations are too complex to be presented here.

A. External Forces

1. Kite Lift and Drag

The kite is assumed to be controlled by manipulating its angle of attack and roll angle. Thus, in this study, its attitude dynamics are ignored. This is the approach that was taken in Refs. 26 and 27, and is also the approach currently used for trajectory optimization for aircraft. A more detailed kite model based on a series of flat plates hinged at the leading edge is presented in Refs. 29 and 30. The incorporation of more representative kite models into the system model presented here is the subject of future research.

The lift and drag forces due to the kite are derived using a velocity coordinate system, as shown in Fig. 4.

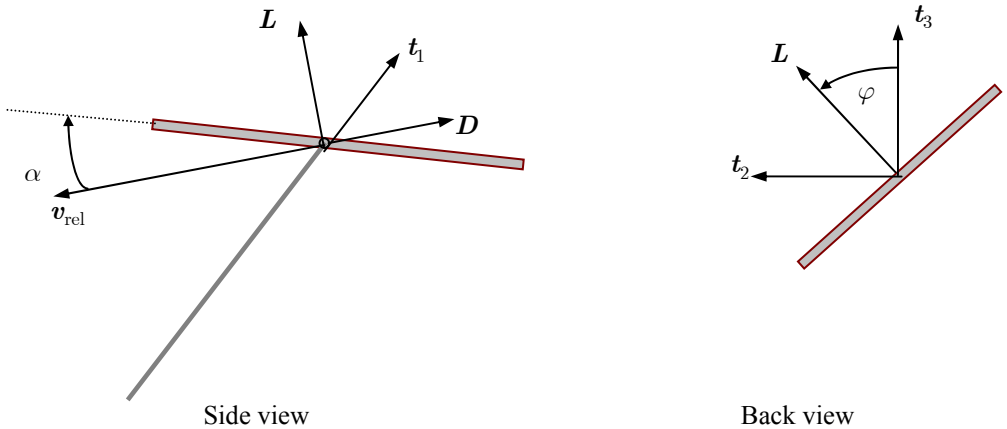

Side view Back view

Fig. 4 Lift and drag forces on kite.

The vector in the inertial frame that defines the plane containing the drag force and the velocity vector is given by

$$\boldsymbol{t}_2 = \frac{\boldsymbol{t} \times \boldsymbol{v}_{\text{rel}}}{\left| \boldsymbol{t} \times \boldsymbol{v}_{\text{rel}} \right|} \tag{14}$$

where $\boldsymbol{t} = [\sin\theta\cos\phi\cos\gamma - \sin\phi\sin\gamma, \sin\theta\cos\phi\sin\gamma + \sin\phi\cos\gamma, \cos\theta\cos\phi]$ is a vector tangential to the cable, $\boldsymbol{v}_{\text{rel}} = \dot{\boldsymbol{R}}_k - \boldsymbol{v}_w$ is the kite velocity relative to the wind, and $\boldsymbol{v}_w$ is the wind vector. The lift force, when the velocity roll angle is zero, is parallel to the vector

$$\boldsymbol{t}_3 = \frac{\boldsymbol{v}_{\text{rel}} \times \boldsymbol{t}_2}{\left| \boldsymbol{v}_{\text{rel}} \times \boldsymbol{t}_2 \right|} \tag{15}$$

Hence, the lift and drag force vectors are defined according to

$$\boldsymbol{L} = \frac{1}{2}\rho C_L S \left| \boldsymbol{v}_{\text{rel}} \right|^2 \left(\boldsymbol{t}_2 \sin\varphi + \boldsymbol{t}_3 \cos\varphi \right), \qquad \boldsymbol{D} = -\frac{1}{2}\rho C_D S \left| \boldsymbol{v}_{\text{rel}} \right| \boldsymbol{v}_{\text{rel}} \tag{16}$$

The lift and drag forces are converted into generalized forces by means of the principle of virtual work, i.e.,

$$Q_\gamma = (\boldsymbol{L}+\boldsymbol{D})\cdot\frac{\partial \boldsymbol{R}_k}{\partial \gamma}, Q_\theta = (\boldsymbol{L}+\boldsymbol{D})\cdot\frac{\partial \boldsymbol{R}_k}{\partial \theta}, Q_\phi = (\boldsymbol{L}+\boldsymbol{D})\cdot\frac{\partial \boldsymbol{R}_k}{\partial \phi}, Q_L = (\boldsymbol{L}+\boldsymbol{D})\cdot\frac{\partial \boldsymbol{R}_k}{\partial L} \tag{17}$$

It should be noted that the roll angle has been arbitrarily defined to be relative to the local tether direction, rather than relative to the inertial axes.

2. Torque Due to Power Generation

When the rotating shaft is used to generate power, it creates a torque that opposes the motion. This torque is modeled as a function of the power level, P. The power level is related to the torque and the instantaneous angular velocity via

$$P = \mathcal{T}\dot{\gamma} \tag{18}$$

Hence, for a given power output, the dissipative torque on the shaft is computed as

$$\mathcal{T} = P/\dot{\gamma} \tag{19}$$

where for simplicity we have assumed a perfectly efficient process. This does not alter the dynamics in any way. The contribution of this torque to the dynamics is computed as

$$Q_\gamma = -\mathcal{T} \tag{20}$$

In reality, there will be friction in the system that will also dissipate rotational energy. However, this is ignored for the study undertaken here.

III. On Kite Dynamics and Estimation

For any of the proposed kite energy systems to become a reality, it will be necessary to develop sophisticated control systems for maneuvering the kite(s). This means that a reliable model of the kite dynamics will be required. A series of data gathering tests with the kite remotely piloted by a joystick has been undertaken by Delft University. At the time of writing, initial tests were conducted that measured the inputs to the kite (attachment point positions),[29] as well as the tether tension vector via a ground based load cell. In order to generate useful kite characteristics, the effect of the tether dynamics must first be removed from the results. This section briefly describes the filtering process used to achieve this. The filtering approach is directly applicable to the rotating kite used in this paper.

A. Coupled Kite and Tether Dynamics

A similar model to that derived in Section II of this paper is used as the process model for the tether/kite system, except that tether mass and drag are taken into consideration. The tether is modeled as a straight inelastic rod with uniform mass. The tether ground station is stationary and the wind direction is assumed to be constant. Details of the tether modeling can be found in Ref. 27. To filter the results, we seek to separate out the effects of the tether from the kite. Hence, we model the kite as a point mass subject to forces in the inertial x, y, and z-directions. These forces and the wind speed are treated as Gaussian white noise processes. The goal of the filter is to take the tension measurements and wind speed estimate from the ground station to produce an output of the tether dynamics together with the kite force estimates. An unscented filter is used to perform the filtering due to its ability to converge from very poor initial state estimates.

B. Unscented Filtering

The unscented Kalman filter was developed by Julier and Uhlmann[31] and assumes a discrete time process model of the form

$$\boldsymbol{x}_{k+1} = \boldsymbol{f}(\boldsymbol{x}_k, \boldsymbol{u}_k, \boldsymbol{v}_k, t_k) \tag{21}$$

$$\boldsymbol{y}_k = \boldsymbol{h}(\boldsymbol{x}_k, \boldsymbol{u}_k, \boldsymbol{w}_k, t_k) \tag{22}$$

where $\boldsymbol{x}_k \in \mathbb{R}^{n_x}$ is the system state vector, $\boldsymbol{u}_k \in \mathbb{R}^{n_u}$ is the system control input, $\boldsymbol{y}_k \in \mathbb{R}^{n_y}$ is the system measurement vector, $\boldsymbol{v}_k \in \mathbb{R}^{n_v}$ is the vector of process noise, assumed to be white Gaussian with zero mean and covariance $\boldsymbol{Q}_k \in \mathbb{R}^{n_v \times n_v}$, $\boldsymbol{w}_k \in \mathbb{R}^{n_w}$ is a vector of measurement noise, assumed to be white Gaussian with zero mean and covariance $\boldsymbol{R}_k \in \mathbb{R}^{n_w \times n_w}$. For the results in this paper, the continuous system is converted to a discrete system by means of a fourth-order Runge-Kutta method.

In the following, the process and measurement noise is implicitly augmented with the state vector as follows

$$\boldsymbol{x}_k^a = \begin{bmatrix} \boldsymbol{x}_k \\ \boldsymbol{v}_k \\ \boldsymbol{w}_k \end{bmatrix} \tag{23}$$

The first step in the filter is to compute the set of sigma points as follows

$$\mathcal{X}_{k-1} = \left[\hat{\boldsymbol{x}}_{k-1}^a, \hat{\boldsymbol{x}}_{k-1}^a + \gamma\sqrt{\boldsymbol{P}_k}, \hat{\boldsymbol{x}}_{k-1}^a - \gamma\sqrt{\boldsymbol{P}_k} \right] \tag{24}$$

where $\hat{\boldsymbol{x}}^a$ is the mean estimate of the state vector, $\boldsymbol{P}_k$ is the covariance matrix, and the parameter γ is defined by

$$\gamma = \sqrt{L + \lambda} \tag{25}$$

and $\lambda = \alpha^2(L + \kappa) - L$ is a scaling parameter, with the values of α and κ selected appropriately, and L is the size of the vector $\hat{\boldsymbol{x}}^a$. The sigma points are then propagated through the nonlinear dynamics as follows

$$\mathcal{X}_{k|k-1}^* = \boldsymbol{f}(\mathcal{X}_{k-1}, \boldsymbol{u}_k, t_k) \tag{26}$$

The predicted mean for the state estimate is calculated from

$$\hat{\boldsymbol{x}}_k^- = \sum_{i=0}^{2L} W_i^{\text{mean}} \mathcal{X}_{i,k|k-1}^* \tag{27}$$

where

$$W_i^{\text{mean}} = \begin{cases} \dfrac{\lambda}{L + \lambda}, & i = 0 \\ \dfrac{1}{2(L + \lambda)}, & i = 1,...,2L \end{cases} \tag{28}$$

The covariance matrix is predicted forward by

$$\boldsymbol{P}_k^- = \sum_{i=0}^{2L} W_i^{\text{cov}} \left[\mathcal{X}_{i,k|k-1}^* - \hat{\boldsymbol{x}}_k^- \right] \left[\mathcal{X}_{i,k|k-1}^* - \hat{\boldsymbol{x}}_k^- \right]^T \tag{29}$$

where

$$W_i^{\text{cov}} = \begin{cases} \dfrac{\lambda}{L+\lambda} + \big(1 - \alpha^2 + \beta\big), & i = 0 \\ \dfrac{1}{2(L+\lambda)}, & i = 1,...,2L \end{cases} \tag{30}$$

Next, the propagated sigma points are augmented by

$$\mathcal{X}_{k|k-1} = \big[\, \mathcal{X}^*_{k|k-1}, \mathcal{X}^*_{k|k-1} + \gamma\sqrt{\boldsymbol{Q}_k}, \mathcal{X}^*_{k|k-1} - \gamma\sqrt{\boldsymbol{Q}_k} \,\big] \tag{31}$$

The augmented sigma points are propagated through the measurement equations

$$\mathcal{Y}_{k|k-1} = \boldsymbol{h}(\mathcal{X}_{k|k-1}, \boldsymbol{u}_k, t_k) \tag{32}$$

The mean observation is obtained by

$$\hat{\boldsymbol{y}}_k^- = \sum_{i=0}^{2L} W_i^{\text{mean}} \mathcal{Y}_{i,k|k-1} \tag{33}$$

The output covariance is calculated using

$$\boldsymbol{P}_k^{yy} = \sum_{i=0}^{2L} W_i^{\text{cov}} \big[\mathcal{Y}_{i,k|k-1} - \hat{\boldsymbol{y}}_k^-\big]\big[\mathcal{Y}_{i,k|k-1} - \hat{\boldsymbol{y}}_k^-\big]^T \tag{34}$$

The cross-correlation matrix is determined from

$$\boldsymbol{P}_k^{xy} = \sum_{i=0}^{2L} W_i^{\text{cov}} \big(\mathcal{X}_{i,k|k-1} - \hat{\boldsymbol{x}}_k^-\big)\big(\mathcal{Y}_{i,k|k-1} - \hat{\boldsymbol{y}}_k^-\big)^T \tag{35}$$

The gain for the Kalman update equations is computed from

$$\mathcal{K}_k = \boldsymbol{P}_k^{xy}(\boldsymbol{P}_k^{yy})^{-1} \tag{36}$$

The state estimate is updated with a measurement of the system $\boldsymbol{y}_k$ using

$$\hat{\boldsymbol{x}}_k = \hat{\boldsymbol{x}}_k^- + \mathcal{K}_k(\boldsymbol{y}_k - \hat{\boldsymbol{y}}_k^-) \tag{37}$$

and the covariance is updated using

$$\boldsymbol{P}_k^+ = \boldsymbol{P}_k^- - \mathcal{K}_k \boldsymbol{P}_k^{yy} \mathcal{K}_k^T \tag{38}$$

These equations are implemented in MATLAB and the filtering process is performed offline. In the future, the filter will be used online to produce estimates in real-time.

C. Numerical Results using Real Kite Measurements

Data was gathered from a flight test where the wind was measured to be steady at approximately 7.5 m/s. The tether length is 68 m, the kite mass is 5 kg, and the tether diameter is 2.5 mm. The drag coefficient of the tether is taken to be 1.2. Numerical results from the flight data are shown in Fig. 5.

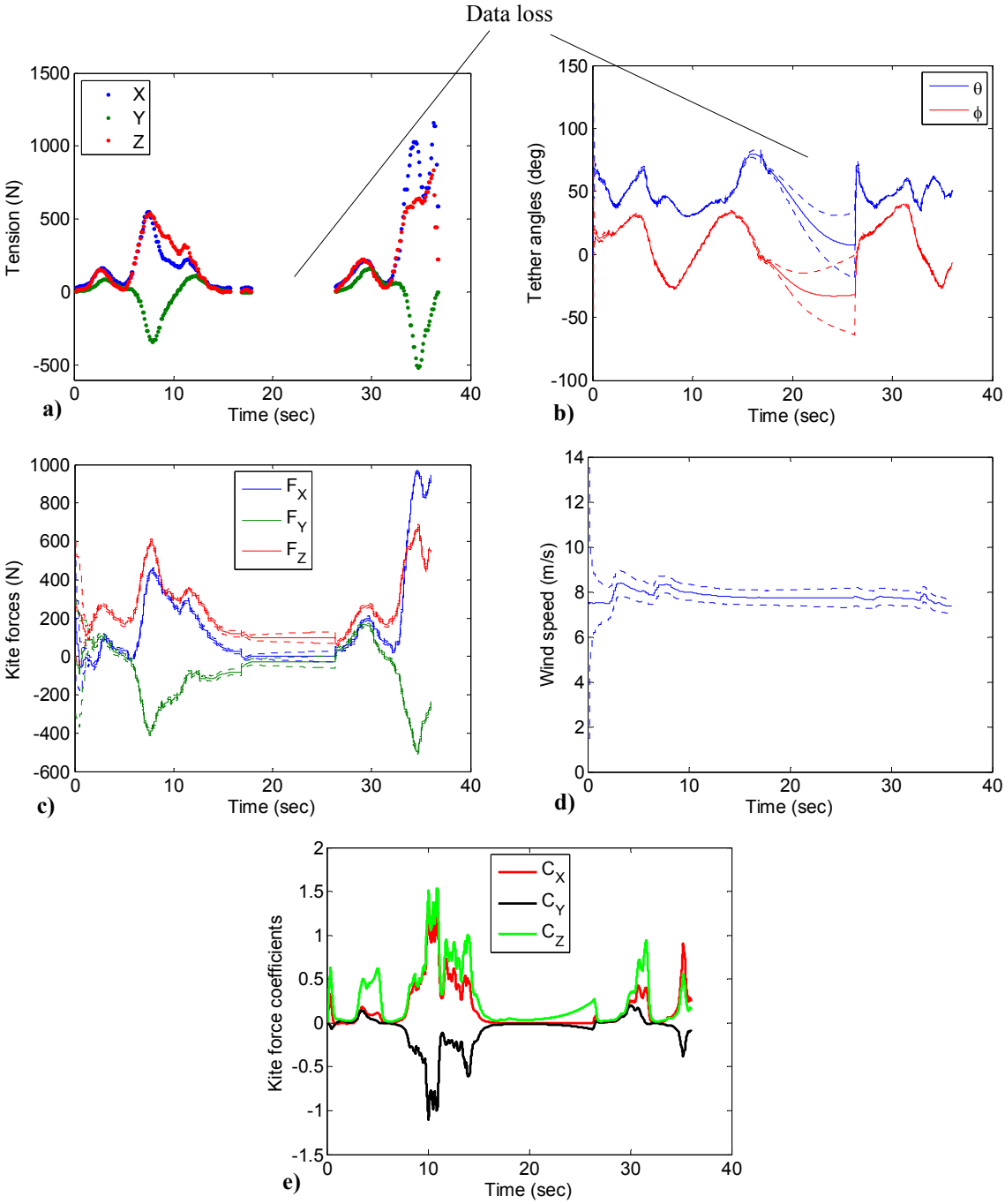

Fig. 5 Filtered estimates of kite data, a) Tension measurements, b) Estimated tether angles and 3σ-covariance bounds, c) Kite forces and 3σ-covariance bounds, d) Wind speed and 3σ-covariance bounds, e) Force coefficients.

Fig. 5a shows the tension measurements made at the ground station. The data was logged intermittently at a rate of approximately 10 Hz, although data loss did occur for an extended period. The results from the filter, which

predicts at a rate of 1000 Hz with measurement updates when available, is shown in Fig. 5b. The 3σ bounds as predicted by the filter are also shown (dotted lines). When the measurement data is not available for an extended period, the uncertainty in the tether states grows rapidly, corresponding to the divergence of the predicted trajectory. This is due to the lack of control inputs into the model, since the entire filtering process relies upon the tension measurements. The estimated kite forces are shown in Fig. 5c, which shows that the force estimates remain static without any tension observations. The results illustrate that most of the tension forces are due to the kite. However, the tether does contribute several hundred Newton's of force during maneuvers due to the high relative winds, which is the reason for removing its effect by using the filter. The estimated wind speed is shown in Fig. 5d, which suggests that the wind speed was moderately constant at between 7.5 and 8 m/s. Fig. 5e shows the resulting force coefficients of the kite by using the relative wind speed at the kite location as the nondimensionalization velocity. These estimates show reasonable values for the force coefficients. These results will prove useful in deriving appropriate realistic aerodynamic models for the kite.

IV. Kite Trajectory Optimization

One of the goals of this paper is to examine the ability of the system to generate power. The wind speed and direction is specified and assumed to remain fixed during an optimization. Any fluctuations in the wind speed are assumed to be handled via feedback. However, feedback control for the kite is an important issue. Possible approaches based on receding horizon control were implemented in Ref. 27. The objective is to maximize the average power output of the system, i.e., minimize the cost

$$J = -\frac{1}{t_f}\int_{t_0}^{t_f} P(t) \tag{39}$$

Subject to the dynamical equations given in Eqs. (8), as well as the periodicity constraints

$$\begin{gathered}\gamma(t_f) - \gamma(t_0) = 2\pi, \theta(t_0) = \theta(t_f), \phi(t_0) = \phi(t_f), \alpha(t_0) = \alpha(t_f), \varphi(t_0) = \varphi(t_f) \\ \dot{\gamma}(t_f) = \dot{\gamma}(t_0), \dot{\theta}(t_0) = \dot{\theta}(t_f), \dot{\phi}(t_0) = \dot{\phi}(t_f), \dot{\alpha}(t_0) = \dot{\alpha}(t_f), \dot{\varphi}(t_0) = \dot{\varphi}(t_f)\end{gathered} \tag{40}$$

and the path constraint on the tether tension

$$T \geq T_{\min} \tag{41}$$

The kite pseudo control inputs are constrained as follows

$$\begin{aligned}\alpha_{\min} \leq \alpha \leq \alpha_{\max} \\ \varphi_{\min} \leq \varphi \leq \varphi_{\max} \\ \dot{\alpha}_{\min} \leq \dot{\alpha} \leq \dot{\alpha}_{\max} \\ \dot{\varphi}_{\min} \leq \dot{\varphi} \leq \dot{\varphi}_{\max}\end{aligned} \tag{42}$$

The periodicity constraints ensure that the trajectory repeats each orbit with a period defined by $t_f - t_0$. The initial time is constrained arbitrarily to be 0, and the final time is free to be optimized.

It should be noted that the problem formulated above is the ideal one that we wish to solve. However, in practice it is necessary to augment the problem slightly due to numerical difficulties. Hence, constraints must be placed on the variation of the states, i.e., $\dot{\gamma}_{\min} \leq \dot{\gamma}(t) \leq \dot{\gamma}_{\max}$. This constraint prevents divide by zero in Eq. (19). In addition, the optimization of the power level is achieved by introducing an additional state variable and control input as follows

$$\dot{P} = u(t) \tag{43}$$

The power rate is included in the cost function with a small weight to prevent sudden changes in the power output and dissipative torque.

A. Solution Technique

The Legendre pseudospectral method has its origins in fluid mechanics[32] and was first applied to optimal control problems by Elnagar et al.[33] Since then, various important properties of the method have been shown to exist, such as convergence,[34,35] as well as the commutivity between discretization and dualization under particular conditions.[36] Apart from these developments, the approach yields particularly simple forms for the discretized Jacobian. This is a consequence of approximating the vector field and tangent bundle separately. This has the advantage that analytic derivatives can be derived in a straightforward manner, making real-time computations possible when combined with fast nonlinear programming solvers.

The states and controls are expanded based on Lagrange interpolating polynomials

$$\boldsymbol{x}^N(t) \approx \sum_{j=0}^{N} \boldsymbol{x}_j \phi_j(t), \qquad \boldsymbol{u}^N(t) \approx \sum_{j=0}^{N} \boldsymbol{u}_j \phi_j(t) \tag{44}$$

The coefficients $\boldsymbol{x}_j = \boldsymbol{x}(t_j), \boldsymbol{u}_j = \boldsymbol{u}(t_j)$ in Eq. (44) are the values of the states and controls at the Legendre-Gauss-Lobatto (LGL) points, which are the zeros of the derivative of the N th order Legendre polynomial L_N defined on the interval $\tau \in [-1,1]$. The Lagrange interpolating polynomials are defined by

$$\phi_j(\tau) = \frac{\left(\tau^2 - 1\right)\dot{L}_N(\tau)}{\left(\tau - \tau_j\right)N(N+1)L_N(\tau_j)}, \qquad j = 0,...,N \tag{45}$$

The state derivatives are approximated by analytically differentiating Eq. (44) and evaluating the result at the LGL points with the result expressible in terms of the differentiation matrix $\boldsymbol{D}$, whose components are defined by

$$D_{k,j} = \begin{cases} \dfrac{L_N(\tau_k)}{L_N(\tau_j)}\dfrac{1}{(\tau_k - \tau_j)} & k \neq j \\ -\dfrac{N(N+1)}{4} & k = j = 0 \\ \dfrac{N(N+1)}{4} & k = j = N \\ 0 & \text{otherwise} \end{cases} \tag{46}$$

The derivatives are easily expressed by the following relationship

$$\dot{\hat{\boldsymbol{x}}} \approx \tfrac{1}{\xi}\boldsymbol{D}\hat{\boldsymbol{x}} \tag{47}$$

where $\hat{\boldsymbol{x}} \triangleq [\boldsymbol{x}_0,...,\boldsymbol{x}_N]$ is the discretized state vector across all nodes, and ξ is the transformation metric defined by the relationship between the computational domain τ and the physical time domain t

$$t = \left(t_f - t_0\right)\tau/2 + \left(t_0 + t_f\right)/2 \tag{48}$$

$$\xi \triangleq \frac{\mathrm{d}t}{\mathrm{d}\tau} = \left(t_f - t_0\right)/2 \tag{49}$$

Finally, the integral cost function is discretized via a Gauss-Lobatto quadrature rule so that

$$\int_{t_0}^{t_f} F(t)\ \mathrm{d}t = \xi \int_{-1}^{1} F(t(\tau))\ \mathrm{d}\tau \approx \xi \sum_{j=0}^{N} w_j F(t_j) \tag{50}$$

where w_j are the Legendre-Gauss-Lobatto weights defined by

$$w_j = \frac{2}{N(N+1)} \frac{1}{\left[L_N\left(\tau_j\right)\right]^2}, \quad k = 0,...,N \tag{51}$$

The process mentioned above is automated in the software DIRECT[37] written by the first author. This software is a MATLAB interface to the solver SNOPT,[38] which implements a quasi-Newton algorithm.

V. Numerical Results

A. Nominal system

Optimal power generating trajectories were generated for a nominal configuration where a large rotational inertia of the base generator is assumed to be 10^6 kg.m^2. The radius arm to the attached tether is assumed to be fixed at 10 m. In the trajectories generated in this paper, the tether length is held fixed at 1000 m. Future work should consider the case where the tether length is allowed to vary. The wind profile follows the form defined by $W_x = v_w(1-\exp(-h/900))$, where h is the kite altitude in meters, and v_w is the "wind speed". The air density is assumed to be fixed at 1.225 kg/m^3. The minimum allowable tether tension is 5 N, and the maximum absolute rate of change of angle of attack and roll angle is 5 deg/sec. The maximum angle of attack is 10 deg, and the maximum absolute roll angle is 30 deg. The kite aerodynamic characteristics are assumed to be $C_L = 4.4\alpha$, $C_D = 0.02 + 0.1C_L^2$. The nominal kite area is 25 m^2 with a mass of 50 kg. The wind speed for the nominal profile is 15 m/s. In solving the optimal control problem via numerical methods, it is possible that the solution obtained can be a local minima. Therefore, it is necessary to start the optimization from different initial guesses. Nevertheless, there is no guarantee that any solutions obtained are global.

The nominal optimal trajectory of the kite is shown in Fig. 6. This plot shows the path taken by the kite in inertial coordinates, together with projections of the tether at different instants of time. This illustrates that the optimal trajectory is in the cross-wind direction, with the kite making a series of regular loops. This clearly illustrates that the kite maintains its position in the downwind direction. This is attributable to the large ratio of tether length to lever arm length. Fig. 7a shows the kite angle of attack for the optimal trajectory. The kite operates at close to the maximum angle of attack for most of the trajectory. However, when the lever arm is moving away from the kite position (i.e., into the wind), the angle of attack is lowered to nearly zero. The angle of attack is then increased to a maximum value when the lever arm is approaching the kite. Fig. 7b shows the kite roll angle, which is essentially bang-bang in the angle rate. Fig. 7c shows the variation in energy generated by the system. The results show that the optimal generating cycle is to cease energy generation when the lever arm is directly pointing in the wind direction. The main reason for this can be seen by examining Fig. 7d, which shows that the torque generated by the tether is negative during this period. To minimize this effect, the angle of attack is controlled to reduce the tension to its minimum value, resulting in nearly zero torque from the tether. The average power generated by the system over one cycle is 20.2 kW.

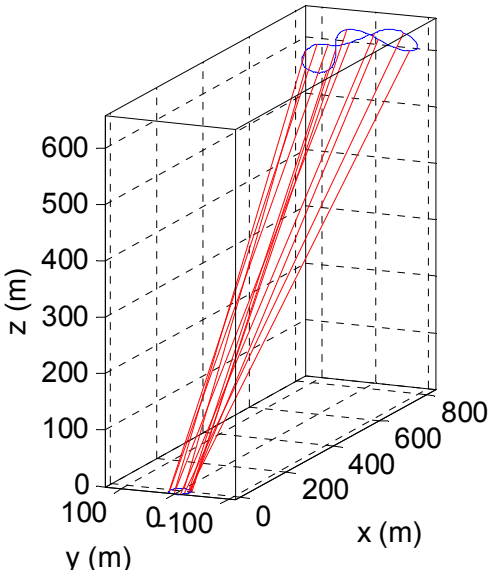

Fig. 6 Optimal power generating kite trajectory for 15 m/s windspeed.

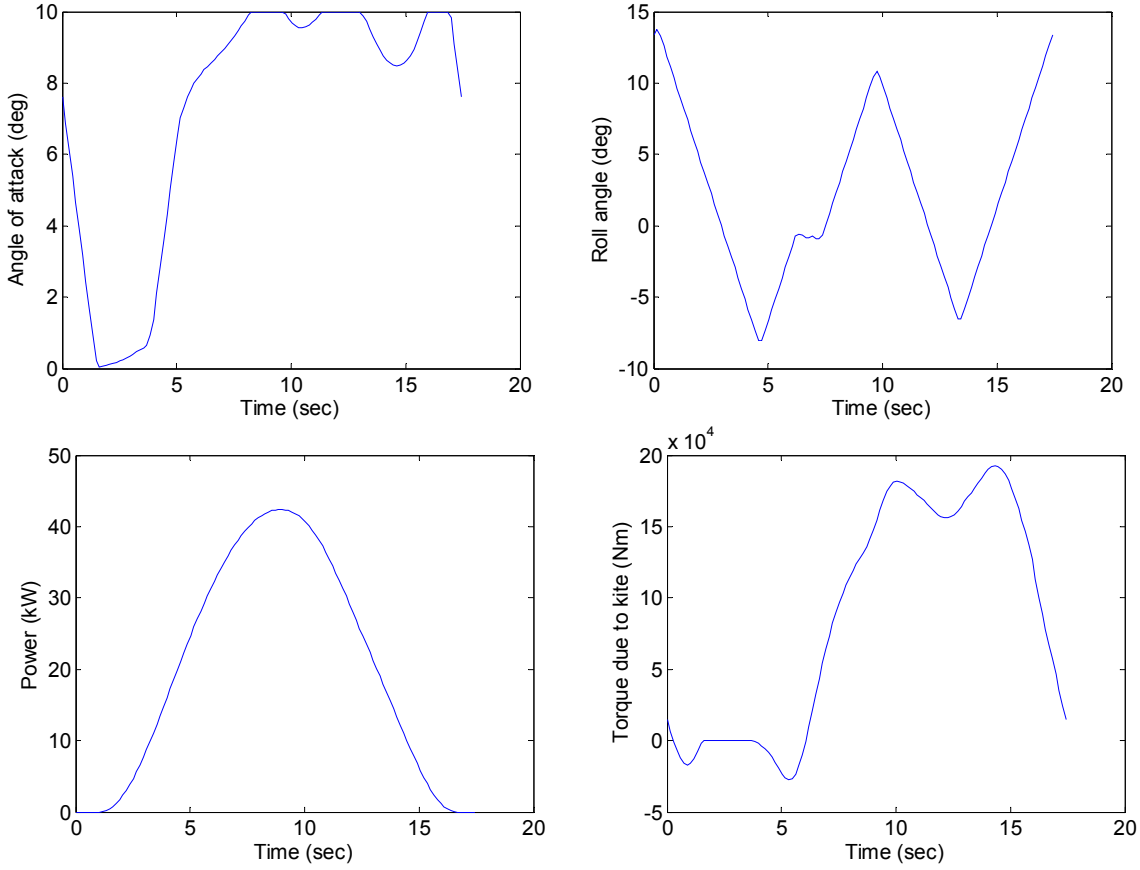

Fig. 7 Optimal trajectories for rotating kite generator in 15 m/s wind, a) Kite angle of attack, b) Kite roll angle, c) Power extracted by generator, d) Torque of tether on lever arm.

B. Effect of kite area

The sensitivity of the optimal solution is first examined with respect to the kite area. The optimal solution for the kite area of 25 m^2 is used as the starting point for the analysis. Fig. 8 shows the kite trajectories in the inertial frame as a function of kite area. The results show that there are two different patterns that the kite flies. For large kite areas, the kite generates larger lift forces, and the kite flies across the wind. Below an area of 18 m^2, the optimal trajectory transitions to an elliptic-like flight pattern with the predominant motion occurring in the vertical direction.

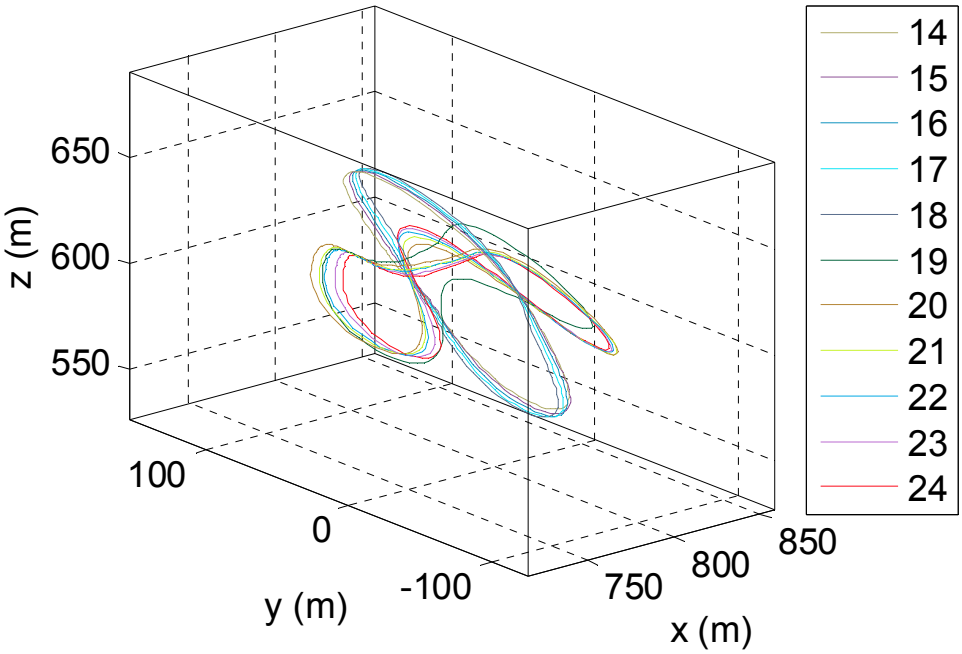

Fig. 8 Optimal kite trajectories as a function of kite area (m^2) in 15 m/s wind.

Fig. 9 shows the optimal angle of attack, roll angle, and power generated by the system. The results show that above 19 m^2, the effect of kite area is relatively minor on the optimal trajectories. The main effect is a change in the optimal cycle period. However, there is a "jump" in the evolution of the trajectories for kite areas below 18 m^2. This causes a significant reduction in the optimal cycling period. The peak power generated per cycle is also significantly reduced. It is interesting to note that the actual angle of attack and roll angle variations are very similar for all trajectories, with an initial drop of the angle of attack when the lever arm passes through the x-axis. Fig. 9c shows that a reduction of the kite area by 40% results in more than a 50 % reduction in the peak power. However, the important measure of efficiency is the average power generated per cycle. This is summarized in Table 1. These results show a nearly direct relationship of the reduction in average power with the percentage reduction in kite area. In other words, the average power generated by the system per cycle in the optimal case is directly proportional to the kite area (assuming all other parameters are held constant).

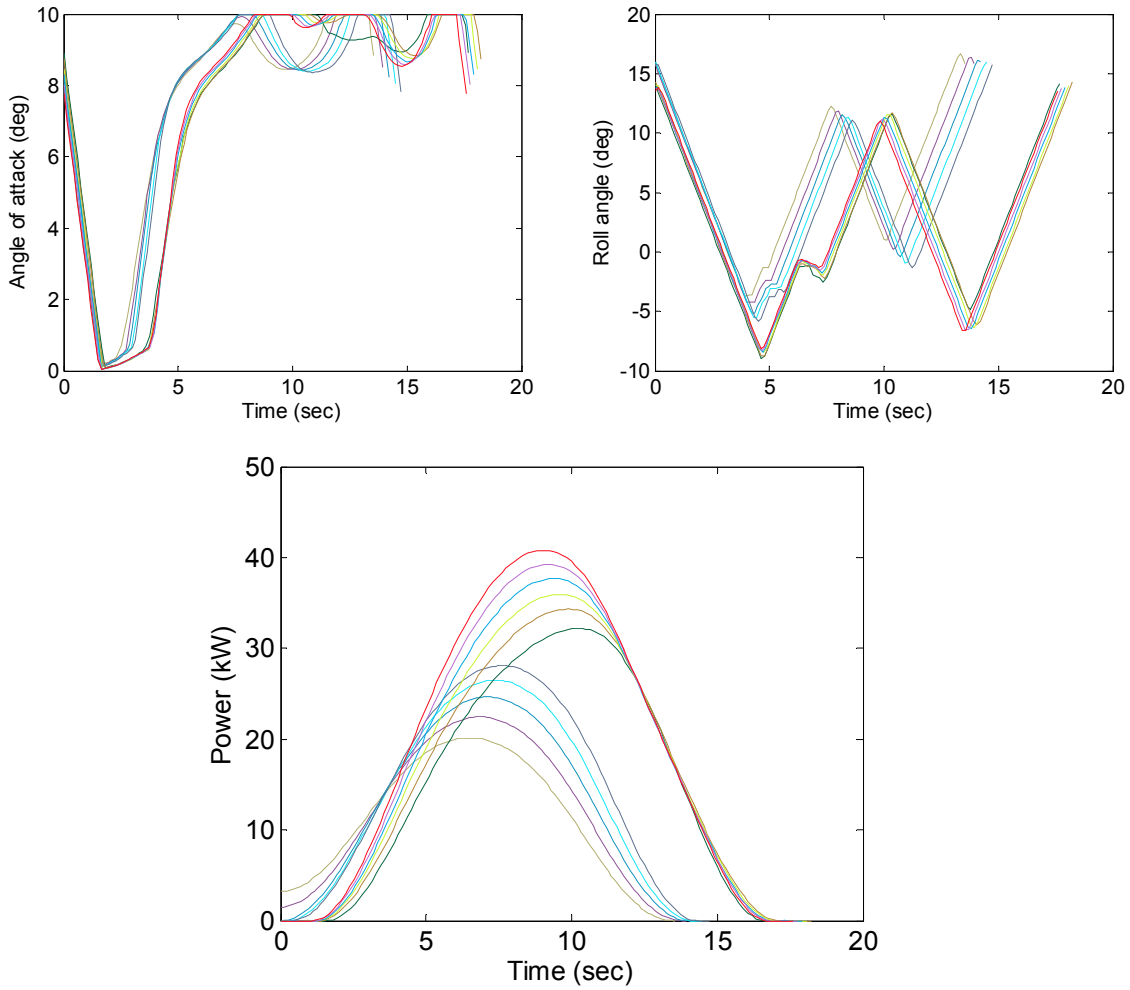

Fig. 9 Optimal trajectories for rotating kite generator as a function of kite area in 15 m/s wind, a) Kite angle of attack, b) Kite roll angle, c) Power extracted by generator.

Table 1 Average power generated as a function of kite area

Kite Area (m^2)	Avg. Power (kW)
14	11.4
15	12.2
16	12.9
17	13.7
18	14.5
19	15.1
20	15.9
21	16.8
22	17.7
23	18.5
24	19.3
25	20.2

C. Effect of wind speed

The final sensitivity study that is conducted is the effect of wind speed on the optimal trajectories. Fig. 10 shows the evolution of the optimal trajectories as the wind speed is varied between 6.5 m/s and 15 m/s. A similar pattern to the effect of kite area is evident in the results. That is, as the wind speed is decreased from the nominal 15 m/s the kite flies less in the cross-wind direction and more in the vertical direction. The transition occurs between wind speeds of 10 and 11 m/s.

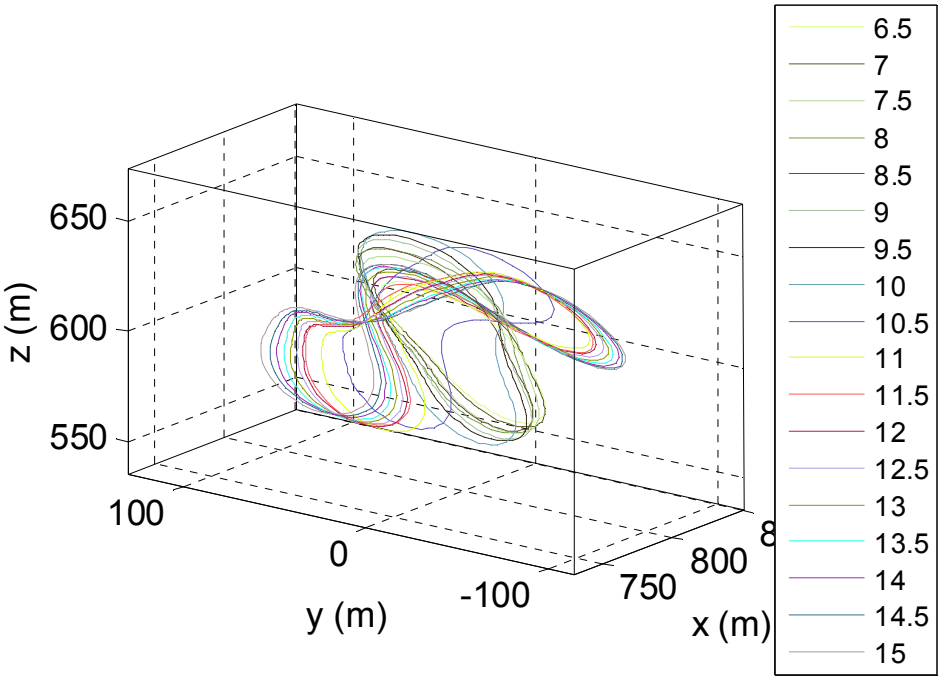

Fig. 10 Optimal kite trajectories as a function of wind speed (m/s).

Fig. 11 shows the optimal variation in kite angle of attack, roll angle, and power generated by the system. The results show that the kite pseudo control inputs are not significantly affected by the wind speed except for low wind speeds (<10 m/s). As the wind speed drops, the minimum demanded kite angle of attack increases, i.e., for a wind speed of 6.5 m/s, the minimum angle of attack is ~6 deg, whereas for 15 m/s the minimum is ~0 deg. This is a result of the minimum tension constraint which maintains the tension above 5 N. The angle of attack cannot be reduced below 6 deg without causing compression in the tether. The variation in power generated over a cycle, shown in Fig. 11c, is significantly influenced by the wind speed. Table 2 summarizes the average power generated per cycle as a function of the wind speed. These results show an approximate cubic relationship between average power and wind speed. The power coefficient of the system, $C_p = P/\left(\frac{1}{2}\rho v_w^3 S\right)$, is approximately constant at a value of 0.4. In other words, for a given kite system, the amount of power generated increases with the cube of the wind speed. This tends to indicate that the trajectories are indeed optimal.

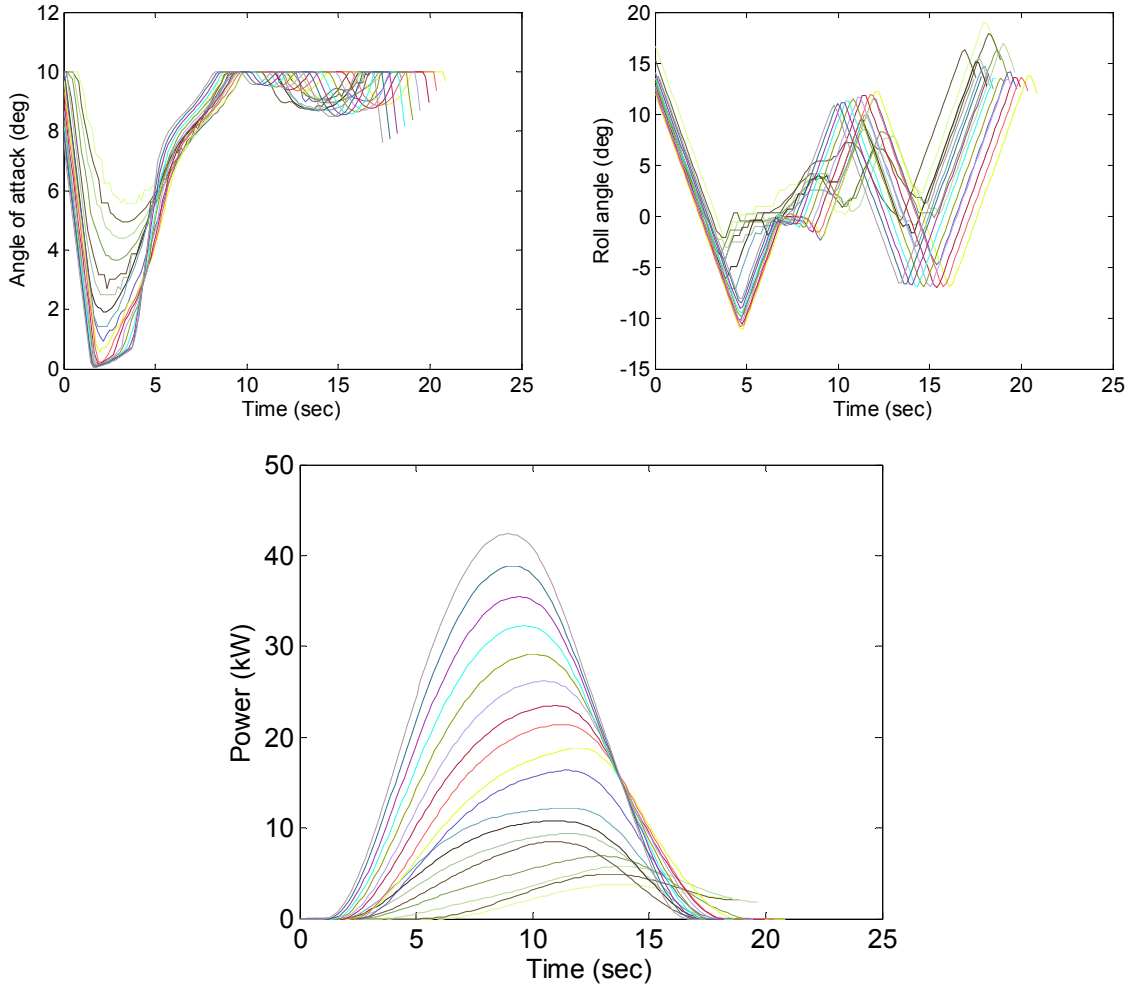

Fig. 11 Optimal trajectories for rotating kite generator as a function of wind speed, a) Kite angle of attack, b) Kite roll angle, c) Power extracted by generator.

Table 2 Effect of wind speed on average power generation per cycle.

Wind speed (m/s)	Avg. Power (kW)
6.5	1.6
7.0	2.1
7.5	2.6
8.0	3.2
8.5	3.8
9.0	4.6
9.5	5.4
10.0	6.2
10.5	7.1
11.0	8.2
11.5	9.4
12.0	10.6
12.5	11.9
13.0	13.4
13.5	14.9
14.0	16.6
14.5	18.3
15.0	20.2

VI. Conclusions

The power generating capability of a rotating vertical axis generator actuated by a kite has been studied using optimal control methodology. A simple model of the system was derived that models the fundamental dynamics of the system. The tether was treated as straight, inelastic and massless. The major limitation of the results is that no tether drag has been included. Results of other studies show that omitting tether drag results in an overestimation of power generation ability, but the nature of the optimal trajectories remain similar. The dynamic model of the system is used to numerically solve for a set of periodic trajectories that maximize the net power generated by the system. The results show a near sinusoidal variation in the power generated over one cycle. The optimal kite trajectory follows a cross-wind pattern for high wind speeds and large kite areas. For lower wind speeds and lower kite areas, the kite tends to move in an elongated ellipse in a plane normal to the wind with the predominant motion occurring in the vertical direction. The average power generated per cycle is proportional to the kite area and the cube of the wind speed.

References

[1]Carpenter, H.G., "Tethered Aircraft Having Remotely Controlled Angle of Attack," US Patent 5,931,416.

[2]Carpenter, H.G., "Tethered Aircraft System for Gathering Energy From Wind," US Patent 6,254,034.

[3]Roberts, B.W., and Shepard, D.H., "Unmanned Rotorcraft to Generate Electricity using Upper Atmospheric Winds," *Australian International Aerospace Congress*, Brisbane, July 2003.

[4]Manalis, M.S., "Airborne Windmills: Energy Source for Communication Aerostats," AIAA Lighter Than Air Technology Conference, AIAA Paper 75-923, July 1975.

[5]Manalis, M.S., "Airborne Windmills and Communication Aerostats," *Journal of Aircraft*, Vol. 13, No. 7, 1976, pp.543-544.

[6]Riegler, G., and Riedler, W., "Tethered Wind Systems for the Generation of Electricity," *Journal of Solar Energy Engineering*, Vol. 106, 1984, pp.177-181.

[7]Riegler, G., Riedler, W., and Horvath, E., "Transformation of Wind Energy by a High-Altitude Power Plant," *Journal of Energy*, Vol. 7, No. 1, 1983, pp.92-94.

[8] Fletcher, C.A.J., and Roberts, B.W., "Electricity Generation from Jet-Stream Winds," *Journal of Energy*, Vol. 3, 1979, pp.241-249.

[9] Fletcher, C.A.J., "On the Rotary Wing Concept for Jet Stream Electricity Generation," *Journal of Energy*, Vol. 7, No. 1, 1983, pp.90-92.

[10]Rye, D.C., "Longitudinal Stability of a Hovering, Tethered Rotorcraft," *Journal of Guidance, Control, and Dynamics*, Vol. 8, No. 6, 1985, pp.743-752.

[11]Fry, C.M., and Hise, H.W., "Wind Driven, High Altitude Power Apparatus," US Patent 4,084,102, April 1978.

[12]Kling, A., "Wind Driven Power Plant," US Patent 4,073,516, Feb. 1978.

[13]Pugh, P.F., "Wind Generator Kite System," US Patent 4,486,669, Dec. 1984.

[14]Biscomb, L.I., "Multiple Wind Turbine Tethered Airfoil Wind Energy Conversion System," US Patent 4,285,481, Aug. 1981.

[15]Watson, W.K., "Airship-Floated Wind Turbine," US Patent 4,491,739, Jan. 1985.

[16]Shepard, D.H., "Power Generation from High Altitude Winds," US Patent 4,659,940, April 1987.

[17]Rundle, C.V., "Tethered Rotary Kite," US Patent 5,149,020, Sept. 1992.

[18]Roberts, B.W., "Windmill Kite," US Patent 6,781,254, Aug. 2004.

[19]Bolonkin, A., "Utilization of Wind Energy at High Altitude," AIAA Paper 2004-5705, Aug. 2004.

[20]Mouton, W.J., and Thompson, D.F., "Airship Power Turbine," US Patent 4,166,596, Sept. 1979.

[21]Ockels, W.J., "Laddermill, a Novel Concept to Exploit the Energy in the Airspace," *Aircraft Design*, Vol. 4, 2001, pp.81-97.

[22]Meijaard, J.P., Ockels, W.J., and Schwab, A.L., "Modelling of the Dynamic Behaviour of a Laddermill, A Novel Concept to Exploit Wind Energy," Proceedings of the Third International Symposium on Cable Dynamics, Norway, Aug. 1999, pp.229-234.

[23]Lansdorp, B., and Ockels, W.J., "Comparison of Concepts for High-Altitude Wind Energy Generation with Ground Based Generator," Proceedings of the NRE 2005 Conference, Beijing, China, pp.409-417.

[24]Lansdorp, B., Remes, B., and Ockels, W.J., "Design and Testing of a Remotely Controlled Surfkite for the Laddermill," World Wind Energy Conference, Melbourne, Australia, Nov. 2005.

[25]Lansdorp, B., and Williams, P., "The Laddermill - Innovative Wind Energy from High Altitudes in Holland and Australia," Paper presented at Wind Power 2006, Adelaide, Australia, September 2006.

[26]Williams, P., "Optimal Wind Power Extraction with a Tethered Kite," AIAA Guidance, Navigation, and Control Conference, Keystone, Colorado, 21-24 August 2006, AIAA Paper 2006-6193.

[27]Williams, P., Lansdorp, B., and Ockels, W., "Optimal Cross-Wind Towing and Power Generation with Tethered Kites," AIAA Guidance, Navigation and Control Conference, Aug. 2007.

[28]Loyd, M.L., "Crosswind Kite Power," *Journal of Energy*, Vol. 4, No. 3, 1980, pp.106-111.

[29]Williams, P., Lansdorp, B., and Ockels, W., "Flexible Tethered Kite with Moveable Attachment Points, Part I: Dynamics and Control," AIAA Atmospheric Flight Mechanics Conference, Aug. 2007.

[30]Williams, P., Lansdorp, B., and Ockels, W., "Flexible Tethered Kite with Moveable Attachment Points, Part II: State and Wind Estimation," AIAA Atmospheric Flight Mechanics Conference, Aug. 2007.

[31]Julier, S.J., Uhlmann, J.K., and Durrant-Whyte, H., "A New Approach for Filtering Nonlinear Systems," in *Proceedings of the American Control Conference*, 1995, pp. 1628–1632.

[32]Canuto, C., Hussaini, M.Y., Quarteroni, A., and Zang, T., *Spectral Methods in Fluid Dynamics*, Springer-Verlag, New York, 1988.

[33]Elnagar, J., Kazemi, M.A., and Razzaghi, M., "The Pseudospectral Legendre Method for Discretizing Optimal Control Problems," *IEEE Transactions on Automatic Control*, Vol. 40, No. 10, 1995, pp.1793-1796.

[34]Gong, Q., Ross, I.M., Kang, W., and Fahroo, F., "Convergence of Pseudospectral Methods for Constrained Nonlinear Optimal Control Problems," *Intelligent Systems and Control*, Series on Modelling, Identification and Control, Acta Press, Calgary, Canada, 2004.

[35]Gong, Q., Ross, I.M., Kang, W., and Fahroo, F., "Dual Convergence of the Legendre Pseudospectral Method for Solving Nonlinear Constrained Optimal Control Problems," *Proceedings of the Intelligent Systems and Control Conference*, Nov. 2005, Paper 497-110.

[36]Ross, I.M., and Fahroo, F., "Legendre Pseudospectral Approximations of Optimal Control Problems," *Lecture Notes in Control and Information Sciences*, Vol. 295, Springer-Verlag, New York, pp.327-342.

[37]Williams, P., "User's Guide to DIRECT Version 2.00," Technical Report TP-07.03.01, Melbourne, Australia.

[38]Gill, P.E., Murray, W., and Saunders, M.A., "SNOPT: An SQP Algorithm for Large-Scale Constrained Optimization," *SIAM Journal on Optimization*, Vol. 12, No. 4, 2002, pp.979-1006.